PERGAMON

International Journal of Heat and Mass Transfer 42 (1999) 35–47

International Journal of HEAT and MASS TRANSFER

Mixed convection heat transfer in a radially rotating square duct with radiation effects

Wei-Mon Yan*, Hung-Yi Li, David Lin

Department of Mechanical Engineering, Huafan University, Shih Ting, Taipei, Taiwan 22305, R.O.C.

Received 14 August 1997; in final form 6 April 1998

Abstract

The interaction of thermal radiation with laminar mixed convection for a gray fluid in a radially rotating square duct is numerically studied. The integro-differential radiative transfer equation is solved by the discrete ordinates method. The coupled momentum and energy equations are solved by the DuFort–Frankel numerical scheme. Results are presented in a radially rotating square duct over a wide range of the governing parameters. The effects of rotation-induced buoyancy and thermal radiation on the developments of velocity, temperature, friction factor and Nusselt number are examined in detail. The axial variations of the *fRe* and *Nu* are characterized by a decay near the entrance due to the entrance effect, but the decay is attenuated by the onset of the secondary flow. The predictions also demonstrate that the radiation presents significant effects on the axial distributions of the total Nusselt number Nu_t and tends to reduce the centrifugal buoyancy effects. In addition, the heat transfer rate increases with the decrease in the conduction-to-radiation parameter N_c.

Nomenclature

a width or height of a square duct, respectively [m]
f friction factor, $2\bar{\tau}_w/(\rho\bar{w}^2)$
G, G^* dimensional and dimensionless incident radiation, $G^* = G/(4\bar{n}^2/\sigma T_w^4)$
Gr_Ω rotational Grashof number, $(\bar{\Omega}^2 a)\beta(T_w - T_o)a^3/v^2$
$\bar{h}$ circumferentially averaged heat transfer coefficient [W m^{-2} °C^{-1}]
h_x locally averaged heat transfer coefficient [W m^{-2} °C^{-1}]
I, J number of finite difference divisions in X and Y directions, respectively
k thermal conductivity [W m^{-1} K^{-1}]
m, m' direction of the discrete ordinates
n, N direction coordinate normal to the duct wall
$\bar{n}$ refractive index
N^* order of the phase function
N_c conduction-to-radiation parameter, $k\bar{\beta}/(4\bar{n}^2\sigma T_w^3)$
Nu peripherally averaged Nusselt number, $\bar{h}a/k$
Nu_c convective Nusselt number
Nu_r radiative Nusselt number
Nu_t total Nusselt number, $Nu_t = Nu_c + Nu_r$
$p_{m'}$, P_m dimensional and dimensionless dynamic pressure, respectively
$\bar{p}$ cross-sectional mean pressure, kPa
$\bar{P}$ dimensionless cross-sectional mean pressure
P' perturbation term about the mean pressure $\bar{P}$
P_n Legendre polynomial
Pr Prandtl number, v/α
q_c convective heat flux
q_r radiation heat flux
q_t total heat flux
Q_r dimensionless radiation flux
Re Reynolds number, $\bar{w}a/v$
Ro rotational number, $\bar{\Omega}a/\bar{w}$
T temperature [°C]
T_o inlet temperature [°C]
T_r ratio of inlet temperature and wall temperature, T_o/T_w
T_w wall temperature [°C]
u, v, w velocity components in x, y and z directions, respectively [m s^{-1}]
U, V, W dimensionless velocity components in X, Y and Z directions, respectively
$\bar{w}$ inlet mean velocity [m s^{-1}]
x, y, z rectangular coordinate [m]

* Corresponding author. E-mail:wmyan@huafan.hfu.edu.tw

0017–9310/98 $19.00
PII: S0017–9310(98)00147–1

X, Y, Z dimensionless rectangular coordinate, $X = x/a$, $Y = y/a$, $Z = z/a$
z_o, Z_o dimensional and dimensionless distance from rotational axis to inlet, respectively
∇^* dimensionless gradient operator.

Greek symbols
α thermal diffusivity [$m^2\ s^{-1}$]
β coefficient of thermal expansion
$\bar{\beta}$ extinction coefficient
ε_w wall emissivity
θ dimensionless temperature, T/T_w
θ_o dimensionless temperature ratio, T_o/T_w
μ, η, ζ direction cosines
ν kinematic viscosity [$m^2\ s^{-1}$]
ξ dimensionless vorticity in axial direction
ρ density [$kg\ m^{-3}$]
σ Stefan–Boltzman constant
$\bar{\sigma}$ scattering coefficient
τ optical thickness
τ_w wall shear stress [kPa]
ψ dimensionless radiation intensity, $\pi I/(\bar{n}^2\sigma T_w^4)$
ϕ scattering phase function
ω single scattering albedo
$\vec{\Omega}, \vec{\Omega}'$ outward and inward direction of radiation
$\bar{\Omega}$ angular velocity of rotation [s^{-1}].

Subscripts
b bulk fluid quantity
c convective
o condition at inlet
r radiative
w value at wall.

Superscript
$\bar{}$ averaged value.

1. Introduction

Combined convection and radiation at high temperatures and high heat fluxes has become increasingly important in the analysis and design of coolant passages for the cooling of turbine or rotor blades. When convection and radiation effects are of the same importance, a separate calculation of convection and radiation and their superposition without considering the interaction between them can lead to significant errors in the results, because the presence of thermal radiation in the flow alters the temperature distributions. Hence, momentum, energy and radiation transport equations must be solved simultaneously in order to determine the local velocity, temperature and heat transfer rate, unless radiation is either very strong or very weak.

A vast amount of work, both theoretical and experimental, exists in the literature to study the flow and heat transfer characteristics in rotating channels without thermal radiation effects, as is evident in the recent studies by Morris [1] and Soong and Hwang [2]. Only those relevant to the present work are briefly reviewed here. The effects of Coriolis force on the flow fields in unheated, rotating ducts have been studied in many investigations [3–10]. These investigators have documented the presence of secondary flow due to the Coriolis-induced force. Studies have been made of the flow and heat transfer in rotating ducts without the added complexity of centrifugal buoyancy and thermal radiation [11–15].

The combined effects of Coriolis and centrifugal buoyancy forces on flow and heat transfer have been examined by a number of investigators. A perturbation analysis was performed by Morris [16] and Siegel [17] to investigate the rotation-induced buoyancy effect on the fully-developed flow and heat transfer in rotating ducts. Experimental studies have been made on the rotating ducts with consideration of centrifugal buoyancy effects [18–22]. Laminar flow and heat transfer through rotating channels was performed by Fann et al. [23] and Fann and Yang [24]. In their studies, the centrifugal buoyancy effects are included in the governing equations. But the parameter of centrifugal buoyancy is negligibly small and its effect was not discussed in the presented results. Recently, a detail numerical analysis of mixed convection in radially rotating rectangular ducts was investigated by Yan and Soong [25] and Yan [26]. In their studies, they found that the rotation-induced buoyancy has a significant impact on the characteristics of fluid flow and heat transfer.

It is noted that there are no numerical studies for combined convection and radiation in rotating ducts. This motivates the present study which treats the characteristics of flow and heat transfer in radially rotating square ducts with consideration of rotation-induced buoyancy and thermal radiation effects. The flow is hydrodynamically and thermally developing.

2. Analysis

As a preliminary attempt to study thermal radiation effects, the flow is assumed to be laminar. In reality, the flow in many applications is turbulent. As a result, the turbulent mixed convection flow and heat transfer in radially rotating ducts should be treated with inclusion of radiation effect. This would, however, greatly complicate the analysis. Therefore, the laminar case is treated in this work and is intended to provide a first step toward future work which will investigate the radiation effects on turbulent mixed convection in radially rotating ducts.

Consider a steady and laminar flow through an isothermal square duct rotating at a constant angular speed $\bar{\Omega}$ about an axis normal to the longitudinal direction of

the duct as shown in Fig. 1. A uniform inlet axial velocity $\bar{w}$ and a constant inlet temperature T_o are imposed at the entrance $z=0$. The u, v, and w are the velocity components in the x, y, and z directions, respectively. To facilitate the analysis, a steady and incompressible flow is assumed and the gravitational force is neglected for its small magnitude compared to the rotation-induced centrifugal force. Additionally, the participating gas is assumed to be gray, absorbing, emitting and scattering.

2.1. Governing equations

The pressure gradient and centrifugal force terms in the x- and z-direction momentum equations are:

$$-\partial p/\partial x+\rho\bar{\Omega}^2 x \tag{1a}$$

$$-\partial p/\partial z+\rho\bar{\Omega}^2(z_o+z). \tag{1b}$$

By invoking the Boussinesq approximation, the density variation in the flow can be approximated by

$$\rho=\rho_o[1-\beta(T-T_o)] \tag{2}$$

where ρ_o is the density evaluated at the reference temperature T_o. With a dynamic pressure p_m defined as

$$p_m=p-p_o \tag{3}$$

where

$$-\partial p_o/\partial x=-\rho_o\bar{\Omega}^2 x \tag{4a}$$

$$-\partial p_o/\partial z=-\rho_o\bar{\Omega}^2(z_o+z) \tag{4b}$$

equation (1) may be rewritten as

$$-\partial p_m/\partial x-\rho\beta(T-T_o)\bar{\Omega}^2 x \tag{5a}$$

$$-\partial p_m/\partial z-\rho\beta(T-T_o)\bar{\Omega}^2(z+z_o). \tag{5b}$$

The flow is assumed to be parabolic and a space-averaged pressure $\bar{p}$ is imposed in the momentum equations to prevail at each cross section, thus permitting a decoupling from the pressure p_m in the cross-sectional momentum equations. This 'pressure uncoupling' follows the parabolic-flow practice and, together with the assumption that neither momentum nor heat is diffused in the axial direction by an order of magnitude analysis, permits a marching-integration calculation procedure [14]. To conveniently present the governing equations, the dynamic pressure p_m can be represented as the sum of a cross-section mean pressure $\bar{p}(z)$, which derives the main flow, and a perturbation about the mean, $p'(x,y,z)$, which derives the cross stream flow,

$$p_m=\bar{p}(z)+p'(x,y,z). \tag{6}$$

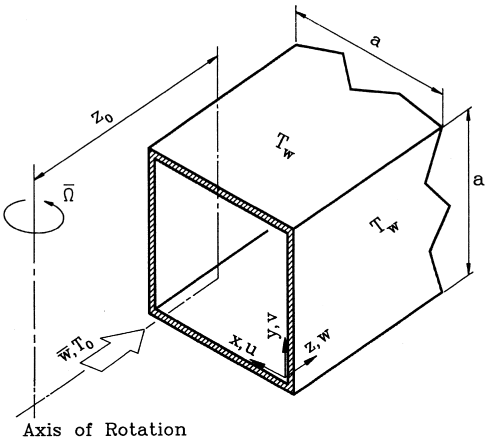

Fig. 1. Schematic diagram of the physical system.

As a final step, dimensionless variables are introduced as follows:

$$X=x/a \quad Y=y/a$$
$$Z=z/a \quad U=u/\bar{w}$$
$$V=v/\bar{w} \quad W=w/\bar{w}$$
$$\bar{P}=\bar{p}/(\rho\bar{w}^2) \quad P'=p'/(\rho\bar{w}^2)$$
$$\theta=T/T_w \quad Re=\bar{w}a/\nu$$
$$Pr=\nu/\alpha \quad Gr_\Omega=(\bar{\Omega}^2 a)\beta(T_w-T_o)a^3/\nu^2$$
$$Ro=\bar{\Omega}a/\bar{w} \quad Z_o=z_o/a$$
$$N_c=k\bar{\beta}/(4\bar{n}^2\sigma T_w^3) \quad \tau=\bar{\beta}a$$
$$\omega=\bar{\sigma}/\bar{\beta} \quad G^*=G/(4\bar{n}^2\sigma T_w^4)$$
$$\theta_o=T_o/T_w \quad T_r=\theta_o \tag{7}$$

With these definitions and the assumptions made earlier, the non-dimensional governing equations are:

continuity equation

$$\partial U/\partial X+\partial V/\partial Y+\partial W/\partial Z=0 \tag{8}$$

x-direction momentum equation

$$U\partial U/\partial X+V\partial U/\partial Y+W\partial U/\partial Z+2Ro\cdot W = -\partial P'/\partial X-Gr_\Omega/Re^2\cdot(\theta-\theta_o)/(1-\theta_o)\cdot X + (\partial^2 U/\partial X^2+\partial^2 U/\partial Y^2)/Re \tag{9}$$

y-direction momentum equation

$$U\partial V/\partial X+V\partial V/\partial Y+W\partial V/\partial Z = -\partial P'/\partial Y+(\partial^2 V/\partial X^2+\partial^2 V/\partial Y^2)/Re \tag{10}$$

z-direction momentum equation

$$U\partial W/\partial X+V\partial W/\partial Y+W\partial W/\partial Z = -\mathrm{d}\bar{P}/\mathrm{d}Z-Gr_\Omega/Re^2\cdot(\theta-\theta_o)/(1-\theta_o)\cdot(Z_o+Z) + (\partial^2 W/\partial X^2+\partial^2 W/\partial Y^2)/Re+2Ro\cdot U \tag{11}$$

energy equation

$$U\partial\theta/\partial X+V\partial\theta/\partial Y+W\partial\theta/\partial Z=[\partial^2\theta/\partial X^2 + \partial^2\theta/\partial Y^2+(1-\omega)\tau^2/N_c\cdot(G^*-\theta^4)]/(Pr\cdot Re). \tag{12}$$

The non-dimensional axial vorticity can be expressed as

$$\xi=\partial U/\partial Y-\partial V/\partial X. \tag{13}$$

The axial vorticity transport equation can be derived from equations (9) and (10) as

$$U\partial\xi/\partial X+V\partial\xi/\partial Y+W\partial\xi/\partial Z+\xi(\partial U/\partial X+\partial V/\partial Y)+(\partial W/\partial Y\cdot\partial U/\partial Z-\partial W/\partial X\cdot\partial V/\partial Z)+2Ro\cdot\partial W/\partial Y=(\partial^2\xi/\partial X^2+\partial^2\xi/\partial Y^2)/Re-Gr_\Omega/Re^2\cdot X\cdot[(\partial\theta/\partial Y)/(1-\theta_o)]. \quad (14)$$

The equations of the transverse velocity components (U, V) can be derived from the continuity equation (8), and the definition of axial vorticity, equation (13), as

$$\partial^2U/\partial X^2+\partial^2U/\partial Y^2=\partial\xi/\partial Y-\partial^2W/\partial X\partial Z \quad (15)$$

$$\partial^2V/\partial X^2+\partial^2V/\partial Y^2=-\partial\xi/\partial X-\partial^2W/\partial Y\partial Z. \quad (16)$$

The overall mass flow rate at every axial location must be balanced in the duct flow, i.e.,

$$\int_0^1\int_0^1 W\cdot\mathrm{d}X\,\mathrm{d}Y=1. \quad (17)$$

This equation is used to deduce the pressure gradient in the axial momentum equation.

The dimensionless incident radiation G^* must be determined from the solution of the radiative transfer equation given by

$$\mu\partial\psi/\partial X+\eta\partial\psi/\partial Y+\tau\psi=(1-\omega)\tau\theta^4+\frac{\omega\tau}{4\pi}\int_{\Omega'=4\pi}\phi(\Omega',\Omega)\psi\,\mathrm{d}\Omega'. \quad (18)$$

It is worth noting that in order to drop the term $\partial\psi/\partial Z$, the assumption that $\partial q_{rz}/\partial Z\ll\partial q_{rx}/\partial X+\partial q_{ry}/\partial Y$ is required. In equation (18), $\psi=\pi\mathrm{I}/(\bar{n}^2\sigma T_w^4)$ is the dimensionless intensity of radiation at a point (X, Y) in the direction $\vec{\Omega}$ defined by the direction cosines μ, η, and ζ, ω is the single scattering albedo and $\phi(\vec{\Omega},\vec{\Omega})$ is the scattering phase function, which is expressed in terms of Legendre polynomials as

$$\phi(\Omega',\Omega)=\sum_{n=0}^{N^*}a_nP_n(\mu'\mu+\eta'\eta+\zeta'\zeta). \quad (19)$$

For a gray, opaque, diffusively emitting, and reflecting surface, the boundary condition is

$$\psi_w(\Omega)=\varepsilon_w+\frac{(1-\varepsilon_w)}{\pi}\int_{n\cdot\Omega'<0}|n\cdot\Omega'|\psi_w(\Omega')\,\mathrm{d}\Omega',\quad \mathbf{n}\cdot\Omega>0 \quad (20)$$

where ε_w is the wall emissivity; and $\vec{\mathbf{n}}$ is the unit normal vector pointing away from the duct wall into the medium.

Once the dimensionless radiation intensity ψ is known, the dimensionless radiation flux vector and incident radiation are determined from their definitions as

$$Q_r=q_r/(4\bar{n}^2\sigma T_w^4)=1/(4\pi)\cdot\int_{\Omega=4\pi}\Omega\psi\,\mathrm{d}\Omega \quad (21a)$$

$$G^*=G/(4\bar{n}^2\sigma T_w^4)=1/(4\pi)\cdot\int_{\Omega=4\pi}\psi\,\mathrm{d}\Omega. \quad (21b)$$

The boundary conditions for the convective governing equations of this problem are given by

$$U=V=W=0,\quad \theta=1 \text{ at the duct walls} \quad (22a)$$

$$W=1,\quad U=V=\xi=0,\quad \theta=T_r \text{ at the entrance } Z=0. \quad (22b)$$

After the developing velocity and temperature fields are obtained, the computations of the circumferentially averaged friction factor and Nusselt number are of practical interest. Following the conventional definitions, the expression for the product of the peripherally averaged friction factor and Reynolds number fRe can be written based on the axial velocity gradient on the duct wall, i.e.,

$$fRe=2(\overline{\partial W/\partial n})_w. \quad (23)$$

Energy transport from the duct wall to the gas flow in the presence of thermal radiation depends on two related factors: the fluid temperature gradient on the duct wall and the rate of radiative heat exchange.

$$q_t=q_c+q_r=-k\partial T/\partial n+q_r. \quad (24)$$

The local total Nusselt number Nu_t defined as

$$Nu_t=\bar{h}a/k=q_ta/[k(T_w-T_b)] \quad (25)$$

consists of both convection and radiation. It is written as

$$Nu_t=Nu_c+Nu_r \quad (26)$$

where Nu_c and Nu_r are, respectively, the local convective Nusselt number and radiative Nusselt number, and are defined as

$$Nu_c=-(\overline{\partial\theta_w/\partial N})/(1-\theta_b) \quad (27)$$

and

$$Nu_r=(\tau\overline{Q_r}/N_c)/(1-\theta_b). \quad (28)$$

Here, the overbar means the average around the perimeters, the Q_r is the dimensionless radiative heat flux at duct wall, and the bulk temperature θ_b is defined as

$$\theta_b=\int_0^1\int_0^1\theta\cdot W\,\mathrm{d}X\,\mathrm{d}Y. \quad (29)$$

2.2. Governing parameters

The parameters involved in the present problem are the Prandtl number Pr, rotational number Ro, rotational Grashof number Gr_Ω, Reynolds number Re, dimensionless distance from the rotational axis to the inlet Z_o, conduction-to-radiation parameter N_c, optical thickness τ, single scattering albedo ω, wall emissivity ε_w, and temperature ratio of inlet fluid and wall T_r. The Gr_Ω measures the importance of the rotation-induced buoyancy effects. The conduction-to-radiation parameter N_c characterizes the relative importance of conduction with respect to radiation. The effect of radiation is getting strong as the N_c decreases. To conveniently discuss the effects of thermal radiation on mixed convection in a radially rotating square duct, Pr, Z_o, and T_r are fixed to be 0.7, 10

and 0.3, respectively. While the other parameters, Ro, Gr_Ω, Re, N_c, τ, ω and ε_w are selected systematically to investigate their influences.

3. Solution method

In this study, the governing equations are solved by the vorticity–velocity method for three-dimensional parabolic flow [27]. The equations for the unknowns U, V, W, ξ, θ and $\mathrm{d}\bar{P}/\mathrm{d}Z$ are coupled. A numerical finite-difference scheme based on the vorticity–velocity method is used to obtain the solution of equations (11), (12) and (14)–(16). Details of the solution procedures have been described elsewhere [25], and is not repeated here. The solution to the radiative transfer equations is obtained by the S_N or the discrete ordinates method [28–30]. In this approach, the solid angle 4π is discretized into a finite number of directions. The discrete ordinates form of the radiative transfer equation can be obtained by evaluating equation at each of the discrete directions and replacing the integral term by a numerical quadrature to give

$$\mu_m \partial\psi_m/\partial X+\eta_m \partial\psi_m/\partial Y+\tau\psi_m = (1-\omega)\tau\theta^4+\frac{\omega\tau}{4\pi}\sum_{m'} w^*_{m'}\,\phi_{m'm}\psi_m \quad (30)$$

with the boundary conditions,

$$\psi_m=\varepsilon_w+\frac{(1-\varepsilon_w)}{\pi}\sum_{m'}\psi_{m'}|\mu_{m'}|w^*_m, \quad \mu_m>0,\ \mu_{m'}<0,\quad X=0 \quad (31a)$$

$$\psi_m=\varepsilon_w+\frac{(1-\varepsilon_w)}{\pi}\sum_{m'}\psi_{m'}|\mu_{m'}|w^*_m, \quad \mu_m<0,\ \mu_{m'}>0,\quad X=1 \quad (31b)$$

$$\psi_m=\varepsilon_w+\frac{(1-\varepsilon_w)}{\pi}\sum_{m'}\psi_{m'}|\eta_{m'}|w^*_m, \quad \eta_m>0,\ \eta_{m'}<0,\quad Y=0 \quad (31c)$$

$$\psi_m=\varepsilon_w+\frac{(1-\varepsilon_w)}{\pi}\sum_{m'}\psi_{m'}|\eta_{m'}|w^*_m, \quad \eta_m<0,\ \eta_{m'}<0,\quad Y=1 \quad (31d)$$

where subscript m and m' represent the direction of the discrete ordinates, and w^*_m are the quadrature weights. The discrete form of the phase function $\phi_{m'm}$ is given by

$$\phi_{m'm}=\sum_{n=0}^{N^*} a_n P_n(\mu_{m'}\mu_m+\eta_{m'}\eta_m+\zeta_{m'}\zeta_m). \quad (32)$$

The accuracy of the S_N method depends on the choice of the quadrature scheme. In this work, the momentum-matching technique suggested by Carson and Lathrop [31] is applied to calculate the discrete directions and quadrature weights as listed in Table 1. The total number of the discrete directions is 24 when the S_6 scheme is used for a two-dimensional geometry. Equations (30), (31), and (32) are solved using the procedure described by Modest [30] to calculate the dimensionless radiation intensity, radiation flux, and incident radiation.

To examine the grid-dependence of the numerical results, a numerical experiment was carried out with various grid distributions in cross-section plane ($I\times J$) and axial step size (ΔZ). In this study, grids were chosen to be uniform in the cross-sectional direction but non-uniform in the axial direction to account for the uneven variations of velocity and temperature in the entrance region. It was found from Table 2 that the deviations in local total Nusselt number Nu_t calculated with $I\times J=41\times41$ and 61×61 ($\Delta Z=0.01$–0.05) are always less than 5% for $Re=1500$, $Ro=0.05$, $Gr_\Omega=1\times10^4$, $N_c=0.05$, $\tau=1$, $\omega=0$ and $\varepsilon_w=0.5$. Furthermore, the deviation sin Nu_t calculated using $I\times J$ (ΔZ) $=41\times41$ (0.001–0.05) and 41×41 (0.01–0.05) are all less than 1%. Accordingly, the computations involving a $I\times J$

Table 1
The discrete directions and quadrature weights for the S_6 method (one octant only)

m	μ_m	η_m	ζ_m	w^*_m
1	0.948235	0.224556	0.224556	$\pi/6$
2	0.689048	0.689048	0.224556	$\pi/6$
3	0.224556	0.948235	0.224556	$\pi/6$
4	0.689048	0.224556	0.689048	$\pi/6$
5	0.224556	0.689048	0.689048	$\pi/6$
6	0.224556	0.224556	0.948235	$\pi/6$

Table 2
Comparison of local total Nusselt number Nu_t for various grid arrangements for $Pr=0.7$, $Re=1500$, $Ro=0.05$, $Gr_\Omega=1\times10^4$, $N_c=0.05$, $\tau=1$, $\omega=0$, $\varepsilon_w=0.5$, and $T_r=0.3$

$(I\times J)$	Z					
(ΔZ)	2.503	5.005	10.018	20.043	30.018	40.0
61×61 (0.01 ~ 0.05)	10.796	9.575	10.562	12.013	13.096	13.779
41×41 (0.001 ~ 0.05)	10.928	9.706	10.780	12.309	13.488	14.287
41×41 (0.01 ~ 0.05)	10.907	9.700	10.773	12.304	13.487	14.277
41×41 (0.05)	10.849	9.691	10.763	12.289	13.481	14.267
31×31 (0.01 ~ 0.05)	11.140	9.939	11.232	12.914	14.278	16.110

$(\Delta Z) = 41 \times 41$ (0.01–0.05) grid are considered to be sufficiently accurate to describe the flow and heat transfer in a radially rotating square duct. All the results presented in the next section are computed using the latter grid. As a partial verification of the computational procedure, results were initially obtained for convection heat transfer in a radially rotating square duct without thermal radiation effect. The results for heat transfer and friction factor were compared with those of Jen et al. [14] and Fann and Yang [24]. The Nusselt number and friction factor were found to agree within 2%.

4. Results and discussion

Figure 2 depicts a series of iso-velocity distributions in the transverse plane at different axial locations. It should be mentioned that the uniform velocity at the entrance $Z = 0$ corresponds to $W = 1$ in the plots. In the absence of rotation, the W profile is symmetrical with respect to $X = 0.5$ line or $Y = 0.5$ line. The W profiles change along the duct axis, beginning with a square shape at $Z = 0$ and finally taking a parabolic shape further downstream. Once rotation is initiated, all the W profiles shift towards the trailing wall ($X = 0$). Take Fig. 2(a) for example. Near the entrance ($Z = 0.208$), the velocity profile is fairly uniform over the cross section. As the flow develops, the velocity in the core region is accelerated due to the entrance effect. Further downstream, the velocity profile becomes distorted with the maximum velocity toward the trailing wall due to the combined centrifugal buoyancy and Coriolis forces acting in the negative X-direction. It is also noted in Fig. 2(a) that the axial velocity gradient on the trailing wall ($X = 0$) is larger than that on the leading wall ($X = 1$). This implies that the friction factor fRe on the trailing wall is larger than that on the leading wall. Figure 2(b) and (c) present the effects of N_c on the iso-velocity distributions with $Re = 1500$, $Ro = 0.05$, $Gr_\Omega = 10^4$, $\tau = 1$, $\omega = 0$ and $\varepsilon_w = 0.5$. The conduction-to-radiation parameter N_c is defined as the ratio of conduction effect to radiation effect. The influence of radiation is getting strong as the value of N_c is decreased. Compared with Fig. 2(a), we note that the results in Fig. 2(b) and (c) are similar to those without radiation in the region near entrance. But as the gas flow goes downstream, the radiation becomes important. The radiation effect tends to reduce the W near the trailing wall. This implies that the results with the inclusion of radiation would reduce the friction factor at a downstream region.

Plotted in Fig. 3 are the isotherm maps at different axial locations. In line with the wall heating, the temperature in the central portion of the duct increases gradually as the flow moves downstream. A comparison of the temperature profiles with and without radiation reveals that near the inlet the effect of radiation on the thermal development is insignificant. But at the downstream location, radiation effect tends to equalize the temperature in the flow. Close inspection on Fig. 3(b) and (c) shows that as the conduction-to-radiation parameter N_c decreases, the θ becomes flatter. Additionally, the development of temperature profile is faster for a system with a stronger radiation effect ($N_c = 0.02$). This can be understood by recognizing that the radiative heat flux is an additional mode of energy transport and as the magnitude of N_c decreases, the importance of the radiation term in equation (12) increases, relative to the conduction and convection. This causes an increase in the energy transport which leads to flatter temperature profiles.

The effects of conduction-to-radiation parameter N_c on the axial variations of bulk temperature, local friction factor and Nusselt number are presented in Figs 4 and 5, respectively. For comparison purposes, the results without thermal radiation effect are also plotted in Figs 4 and 5, as shown by the dotted lines. From Fig. 4, the bulk temperature distributions were found to be essentially the same as those without radiation when the radiation-convection interaction is weak, such as for the curve of $N_c = 1$. However, when the interaction is intense ($N_c = 0.02$), there is an essential difference. In contrast to the case without radiation, the radiation augments the rate of thermal development so that the θ_b approaches the wall temperature ($\theta = 1$) at a more rapid rate. In Fig. 5(b), both total Nusselt number Nu_t and convective Nusselt number Nu_c are illustrated in the same subplot. The difference between Nu_t and Nu_c at the same position represents the radiative Nusselt number Nu_r. In all cases the total Nusselt number Nu_t with radiation is larger than that without radiation. This is due to two effects. The first is that radiation is additional mechanism for heat transfer through the fluid resulting in an increased heat flux. Secondly, the radiation source term augments the rate of thermal development so that the bulk temperature approaches the wall temperature at a more rapid rate. Both effects act to increase the local total Nusselt number Nu_t. Near the entrance, the Nu_t is raised only by the additional radiative heat flux, while further downstream, the more rapid thermal development contributes when the bulk temperature approaches the wall temperature. An overall inspection on Fig. 5 reveals that near the entrance, the local fRe and Nu fade away monotonically due to the entrance effect. At these positions, the convective effect is predominant. Therefore, the effects of N_c on fRe and Nu are insignificant. But as the flow proceeds downstream, the radiation effect becomes important. The local Nu_c and Nu_t increases with the decrease in the N_c due to the strong radiation effect. But this is not the case for local fRe. At downstream region, the fRe decreases with the decreases in N_c. This is due to the fact that in the presence of radiation, the temperature field becomes relatively flatter, as shown in Fig. 3. The centrifugal buoyancy effect is thus reduced, which in turn, causes a reduction in fRe further downstream.

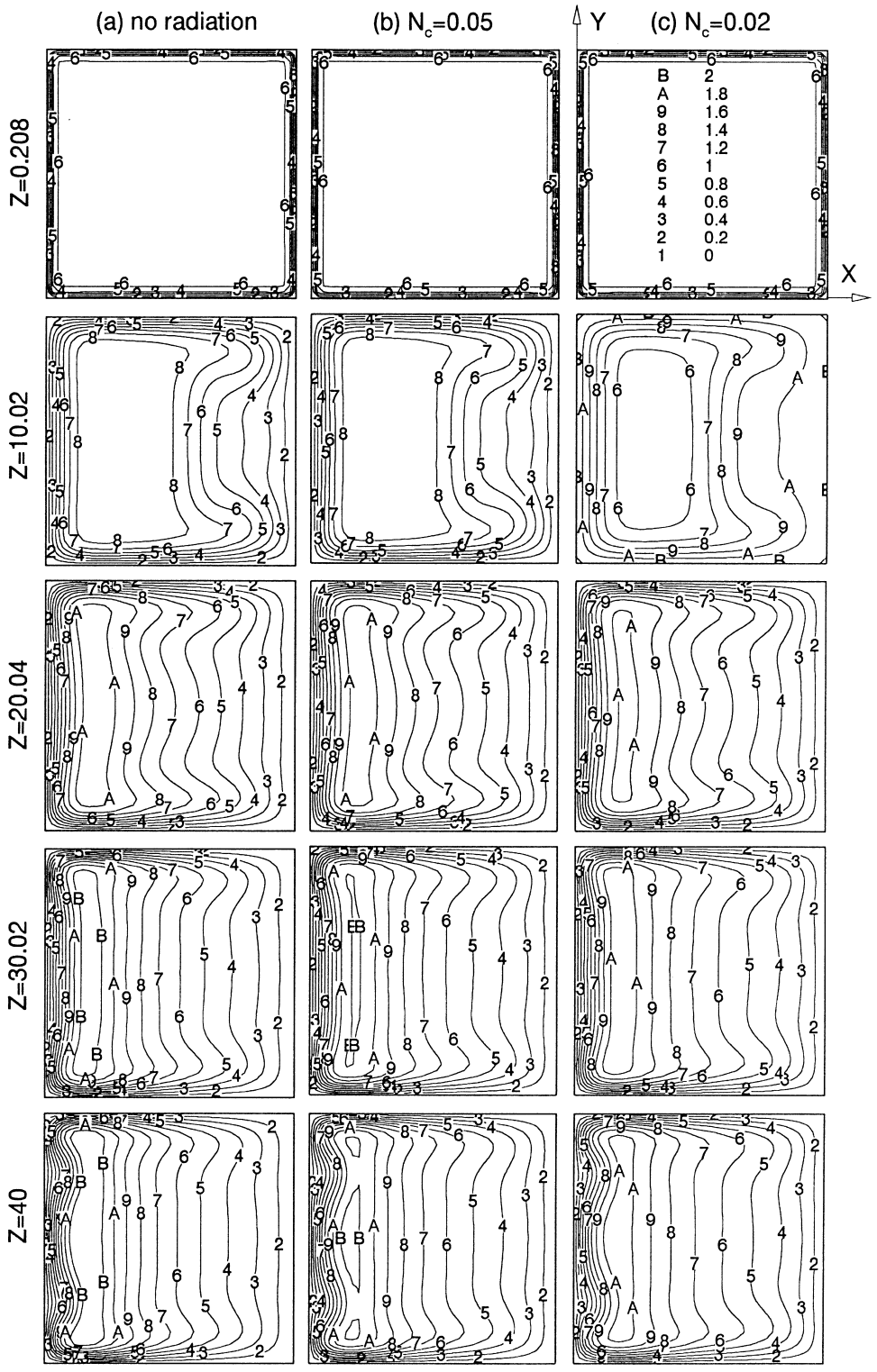

Fig. 2. Iso-velocity maps for $Re = 1500$, $Ro = 0.05$, $Gr_\Omega = 10^4$, $\tau = 1$, $\omega = 0$, $\varepsilon_w = 0.5$ and (a) $N_c \to \infty$ (no radiation), (b) $N_c = 0.05$, (c) $N_c = 0.02$.

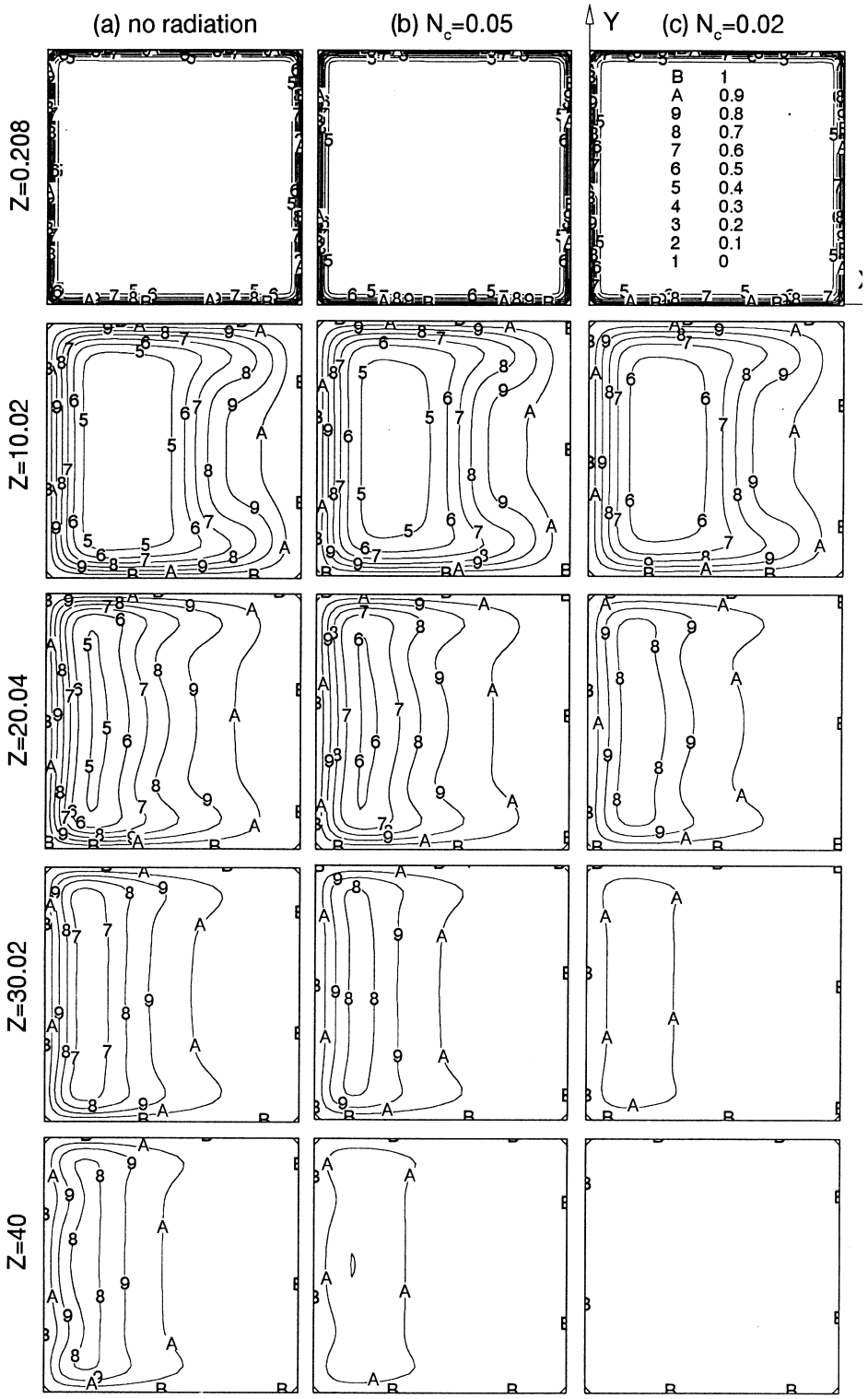

Fig. 3. Isotherm maps for $Re = 1500$, $Ro = 0.05$, $Gr_\Omega = 10^4$, $\tau = 1$, $\omega = 0$, $\varepsilon_w = 0.5$ and (a) $N_c \to \infty$ (no radiation), (b) $N_c = 0.05$, (c) $N_c = 0.02$.

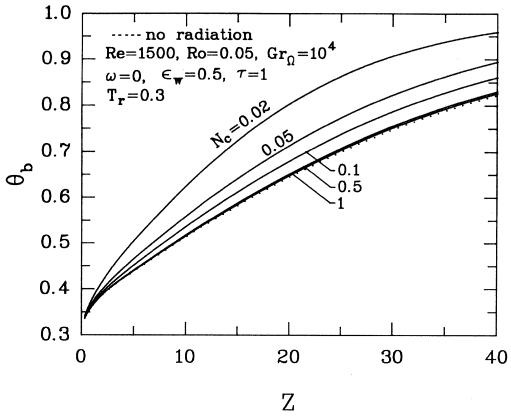

Fig. 4. Effects of N_c on the variations of bulk temperature θ_b for $Re = 1500$, $Ro = 0.05$, $Gr_\Omega = 10^4$, $\tau = 1$, $\omega = 0$, $\varepsilon_w = 0.5$.

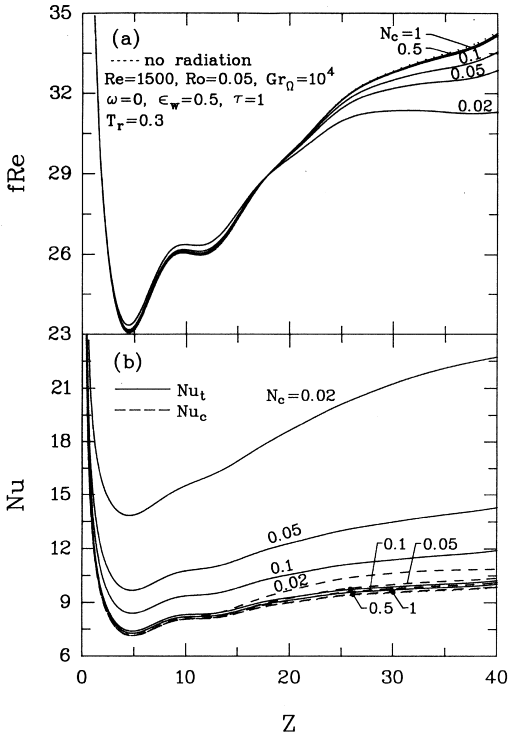

Fig. 5. Effects of N_c on the variations of friction factor and Nusselt number for $Re = 1500$, $Ro = 0.05$, $Gr_\Omega = 10^4$, $\tau = 1$, $\omega = 0$, $\varepsilon_w = 0.5$.

The effects of optical thickness τ on local fRe and Nu are shown in Fig. 6. A strong radiatively participating medium corresponds to a larger optical thickness. It is easy to see that there is more heat released from such

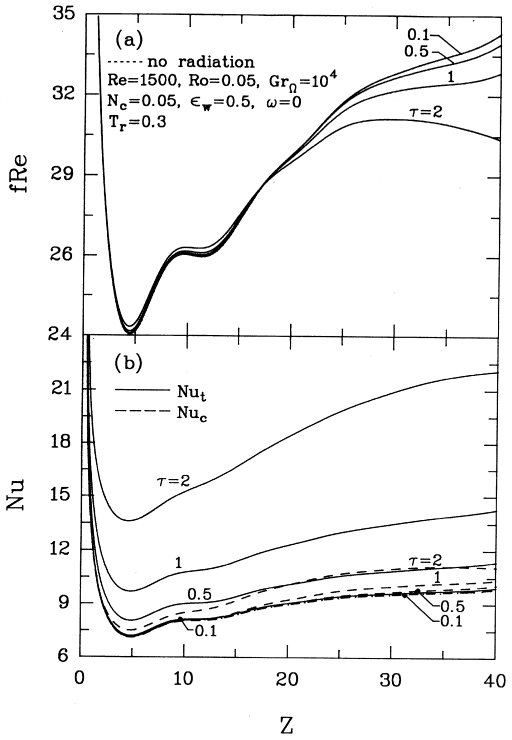

Fig. 6. Effects of τ on the variations of friction factor and Nusselt number for $Re = 1500$, $Ro = 0.05$, $Gr_\Omega = 10^4$, $N_c = 0.5$, $\omega = 0$, $\varepsilon_w = 0.5$.

a medium than from a weak radiatively participating medium. Thus the local Nu_c and Nu_t increases with an increase in τ. Additionally, the radiation has a stronger effect on the local fRe and Nu for a system with a larger τ, as compared with the results of no radiation.

In many applications, scattering processes are important in radiative heat transfer if participates are present in the fluid. Therefore, the effects of single scattering albedo on the fluid flow and heat transfer are of interest. For illustration, the scattering is assumed to be isotropic. Figure 7 demonstrates the influence of single scattering albedo ω on the local fRe and Nu distributions. There is less absorption of radiation by an absorbing and scattering fluid as compared with the nonscattering case ($\omega = 0$). Therefore, the Nu decreases with an increase in ω. Like the results in Fig. 6(a), the local fRe are attenuated due to the radiation effect at downstream region.

The effects of wall emissivity ε_w on the local fRe and Nu are shown in Fig. 8. It is apparent that the local Nu without radiation is lower than those with radiation. The larger the wall emissivity ε_w, the higher the local Nu and fRe at the same position. This is due to the intense interaction between the radiation and convection as the ε_w is increased.

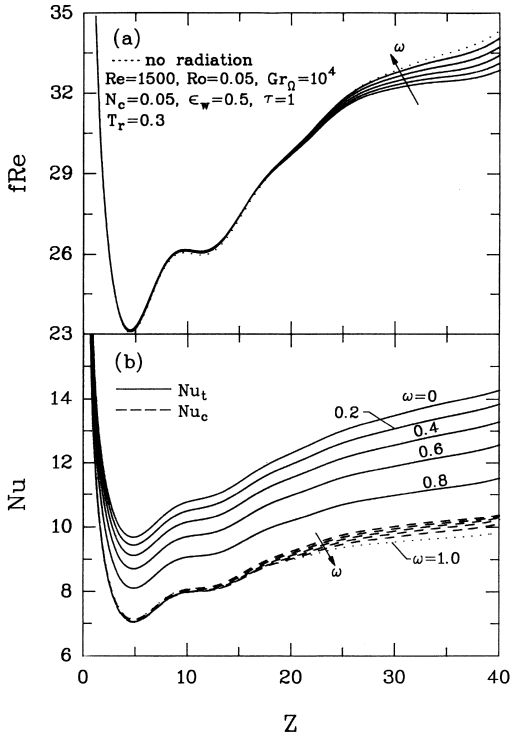

Fig. 7. Effects of ω on the variations of friction factor and Nusselt number for $Re = 1500$, $Ro = 0.05$, $Gr_\Omega = 10^4$, $N_c = 0.05$, $\tau = 1$, $\varepsilon_w = 0.5$.

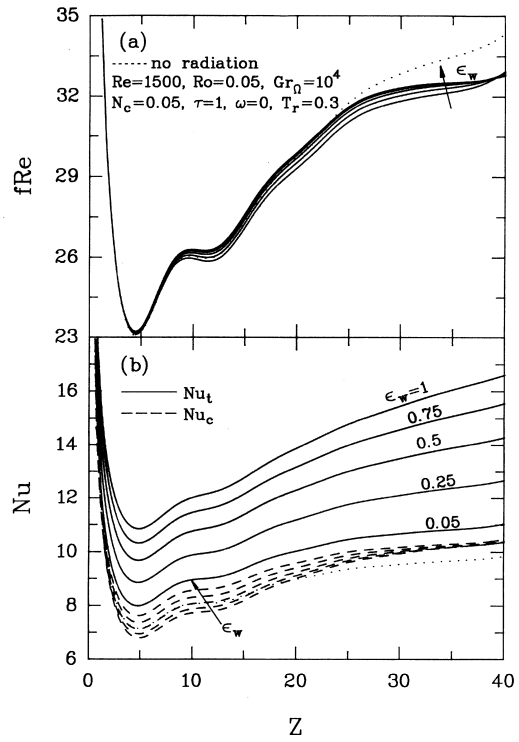

Fig. 8. Effects of ε_w on the variations of friction factor and Nusselt number for $Re = 1500$, $Ro = 0.05$, $Gr_\Omega = 10^4$, $N_c = 0.05$, $\tau = 1$, $\omega = 0$.

Figure 9 presents the axial variations of the circumferentially averaged friction factor fRe and Nusselt number Nu with rotational number Ro as a parameter. In this plot, only the convective Nusselt number Nu_c is presented. The decreases in local values of fRe and Nu_c near the inlet are attributed to the forced-convection entrance effect, and the deviation from the results of stationary duct ($Ro = 0$) is caused by the rotational effects. The entrance and rotational effects are balanced out and a local minimum in fRe (or Nu_c) appears at a position of distance from inlet, which depends upon the value of Ro. Subsequently, the rotational effect dominates over the entrance effect and the fRe (or Nu_c) increases until a local maximum for fRe (or Nu_c) may exist for some cases. It is worth noting that for $Ro = 0.075$ and 0.1, oscillations in the variations of fRe and Nu exist after the first local minimum. This behavior is related to the emergence and decay of the second pair of vortices near the trailing wall. In addition, larger fRe and Nu result for a larger Ro due to the stronger Coriolis force. Comparison of the results between the solid and dotted curves indicates that the effect of radiation on the fRe and Nu are insignificant at the entrance region. But as the flow goes downstream, the radiation becomes important.

In high rotation rates and high wall-to-coolant temperature differences in rotating elements, the centrifugal force may play a very critical role in the flow and heat transfer mechanism. Hence, it is interesting to examine the influence of centrifugal buoyancy on the flow and heat transfer. Figure 10 shows the effects of the centrifugal buoyancy on the fRe and Nu for $Re = 1500$, $Ro = 0.05$, $N_c = 0.05$, $\tau = 1$, $\omega = 0$ and $\varepsilon_w = 0.5$. It is obvious that the centrifugal buoyancy effect decreases the Nu_c as compared with the results of buoyancy-free case ($Gr_\Omega = 0$), and the extent of decrease in Nu_c increases with Gr_Ω. In Fig. 10(a), the effects of centrifugal buoyancy on the fRe are complicated. As $Z < 15$, a larger fRe is noted for a system with a smaller Gr_Ω. But as $Z > 15$, the reverse trend is found. It is also interesting to note in Fig. 10(a) that relative to the results without radiation, the radiation effect would decrease the local fRe. This is due to the fact that the radiation tends to reduce the centrifugal buoyancy effect.

To explore the effect of the through-flow Reynolds number Re on the variations of fRe and Nu_c, Fig. 11 presents the local fRe and Nu_c distributions with

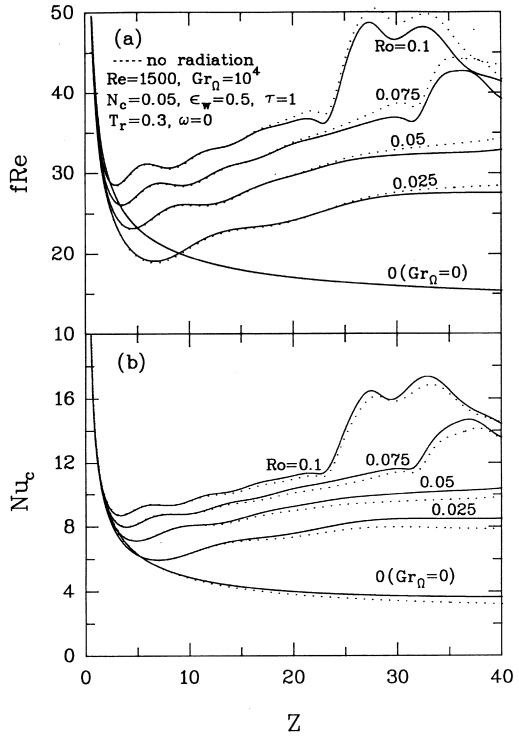

Fig. 9. Effects of Ro on the variations of friction factor and Nusselt number for $Re = 1500$, $Gr_\Omega = 10^4$, $N_c = 0.05$, $\tau = 1$, $\omega = 0$, $\varepsilon_w = 0.5$.

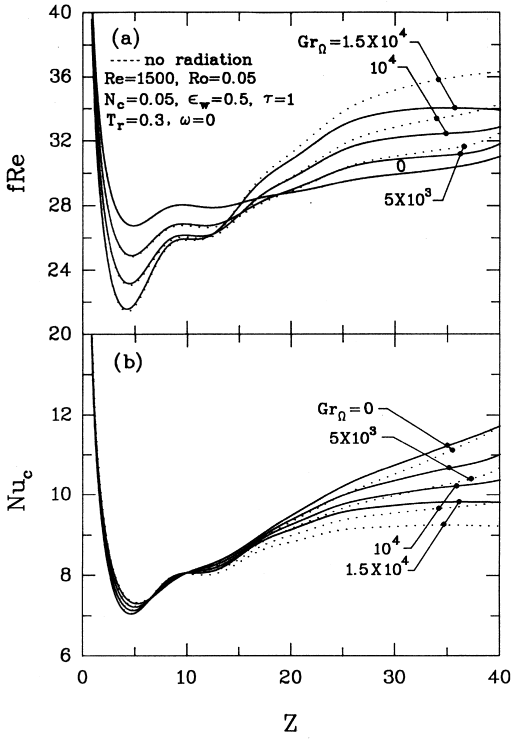

Fig. 10. Effects of Gr_Ω on the variations of friction factor and Nusselt number for $Re = 1500$, $Ro = 0.05$, $N_c = 0.05$, $\tau = 1$, $\omega = 0$, $\varepsilon_w = 0.5$.

Reynolds number as a parameter. As shown in Fig. 11, larger fRe and Nu_c are experienced for a system with a higher Reynolds number Re due to a larger forced-convection effect. It is also found in the separate computation run that the centrifugal buoyancy effect diminishes as the Re increases.

5. Conclusions

In the present work, mixed convection flow and heat transfer in a radially rotating square duct with consideration of rotation-induced buoyancy and thermal radiation effects have been studied numerically. A relatively novel vorticity-velocity method successively solved the three-dimensional parabolic governing equations. The radiative transfer equation was solved by the discrete ordinates method. The effects of the rotational number Ro, rotational Grashof number Gr_Ω, Reynolds number Re, conduction-to-radiation parameter N_c, optical thickness τ, single scattering albedo ω and wall emissivity ε_w on the flow and heat transfer are examined in detail. What follows is a brief summary.

(1) In the presence of radiation, the thermal development develops at a more rapid rate relative to that without radiation.
(2) The axial distributions of Re and Nu are characterized by a drop near the inlet due to the entrance effect, but the decay is reduced by the onset of secondary flow.
(3) The circumferentially averaged friction factor fRe and convective Nusselt number Nu_c are enhanced with an increase in the rotational number Ro and the throughflow Reynolds number Re.
(4) The convective Nusselt number Nu_c are augmented by the radiation effects. Conversely, the fRe is reduced in the presence of radiation at downstream region.
(5) In contrast to the results without radiation, radiation effects augments the Nu_t. And the extent of enhancement in Nu_t increases with a decrease (increase) in N_c or ω (τ or ε_w).

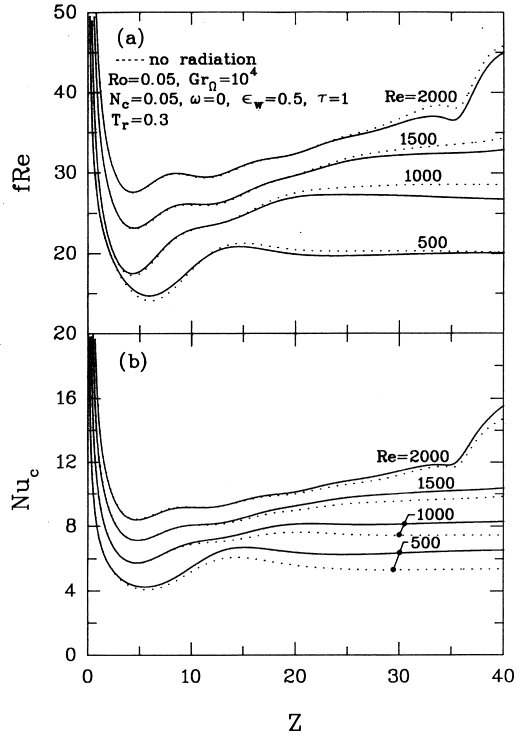

Fig. 11. Effects of *Re* on the variations of friction factor and Nusselt number for $Ro = 0.05$, $Gr_\Omega = 10^4$, $N_c = 0.05$, $\tau = 1$, $\omega = 0$, $\varepsilon_w = 0.5$.

Acknowledgement

The financial support of this research by the National Science Council, R.O.C., under the contract NSC 85-2212-E-211-005 is greatly appreciated.

References

[1] W.D. Morris, Heat Transfer and Fluid Flow in Rotating Coolant Channels. John Wiley and Sons, Chichester, 1981.
[2] C.Y. Soong, G.J. Hwang, Convective heat transfer in radially rotating coolant channels of turbomachinery. Proceedings of Aero. and Astro. Conf., AASRC, Taipei, R.O.C., 16 December 1990.
[3] J.E. Hart, Instability and secondary flow in a rotating channel flow. J. Fluid Mech. 45 (1971) 341–351.
[4] H. Ito, K. Nanbu, Flow in rotating straight pipes of circular cross section. J. Basic Eng. 93 (1971) 383–394.
[5] J. Moore, A wake and eddy in a rotating, radial-flow passage. Part 1: experimental observations. J. Eng. Power 95 (1973) 205–212.
[6] J. Moore, A wake and eddy in a rotating, radial-flow passage. Part 2: flow model. J. Eng. Power 95 (1973) 213–219.
[7] A.K. Majumdar, V.S. Pratap, D.B. Spalding, Numerical computation of flow in rotating ducts. J. Fluid. Eng. 99 (1977) 148–153.
[8] C.G. Speziale, Numerical study of viscous flow in rotating rectangular ducts. J. Fluid Mech. 122 (1982) 251–271.
[9] C.G. Speziale, S. Thangam, Numerical study of secondary flows and roo-cell instabilities in rotating channel flow. J. Fluid Mech. 130 (1983) 377–395.
[10] C.G. Speziale, Numerical solution of rotating internal flows. Lectures in Appl. Math. 22 (1985) 261–289.
[11] Y. Mori, T. Fukada, W. Nakayama, Convective heat transfer in a rotating radial circular pipe (2nd report). Int. J. Heat Mass Transfer 11 (1971) 1807–1824.
[12] V. Vidyanidhi, V.V.S. Suryanarayana, R. Chenchu, An analysis of steady fully developed heat transfer in a rotating straight pipe. J. Heat Transfer 99 (1977) 148–153.
[13] G.J. Hwang, T.C. Jen, Convective heat transfer in rotating isothermal ducts. Int. J. Heat Mass Transfer 33 (1990) 1817–1828.
[14] T.C. Jen, A.S. Lavine, G.J. Hwang, Simultaneously developing laminar convection in rotating isothermal square channels. Int. J. Heat Mass Transfer 35 (1992) 239–254.
[15] T.C. Jen, A.S. Lavine, Laminar heat transfer and fluid flow in the entrance region of a rotating duct with rectangular cross section: the effect of aspect ratio. J. Heat Transfer 114 (1992) 574–581.
[16] W.D. Morris, Flow and heat transfer in rotating coolant channels. High Temperature Turbines, AGARD CP-229, 1977, 38–1 to 38–14.
[17] R. Siegel, Analysis of buoyancy effect on fully developed laminar heat transfer in a rotating tube. J. Heat Transfer 107 (1985) 338–344.
[18] R.J. Clifford, S.P. Harasgama, W.D. Morris, An experimental study of local and mean heat transfer in a triangular-sectional duct rotating in the orthogonal mode. Int. J. Turbo. Jet Engines 2 (1985) 93–106.
[19] K.M. Iskakov, V.A. Trushin, The effect of rotation on heat transfer in the radial cooling channels of turbine blades. Thermal Engineering 32 (1985) 93–96.
[20] J.H. Wagner, B.V. Johnson, T.J. Hajek, Heat transfer in rotating passages with square smooth walls and radial outward flow. J. Turbomachinery 113 (1991) 42–51.
[21] C.Y. Soong, S.T. Lin, G.J. Hwang, An experimental study of convective heat transfer in radially rotating rectangular ducts. J. Heat Transfer 113 (1991) 604–611.
[22] J.C. Han, Y.M. Zhang, Effect of uneven wall temperature on local heat transfer in a rotating square channel with smooth walls and radial outward flow. J. Heat Transfer 114 (1992) 850–858.
[23] S. Fann, W.J. Yang, S. Mochizuki, Transport phenomena in laminar developing flow of rotating heated channels. Proceedings of Fourth Symposium on Transport Phenomena and Dynamics of Rotating Machinery Vol. B (1992) 511–525.
[24] S. Fann, W.J. Yang, Hydrodynamically and thermally developing laminar flow through rotating channel having isothermal walls. Numer. Heat Transfer, Part A 22 (1992) 247–288.
[25] W.M. Yan, C.Y. Soong, Simultaneously developing mixed convection in radially rotating rectangular ducts. Int. J. Heat Mass Transfer 38 (1995) 665–577.

[26] W.M. Yan, Effects of wall transpiration on mixed convection in a radial outward flow inside rotating ducts. Int. J. Heat Mass Transfer 38 (1995) 2333–2342.
[27] K. Ramakrishna, S.G. Rubin, P.K. Khosla, Laminar natural convection along vertical square ducts. Numer. Heat Transfer 5 (1982) 59–79.
[28] W.A. Fiveland, Three-dimensional radiative heat transfer solution by the discrete-ordinates method. J. Thermophysics and heat Transfer 2 (1988) 309–316.
[29] T.Y. Kim, S.W. Baek, Analysis of combined conductive and radiative heat transfer in a two-dimensional rectangular enclosure using the discrete ordinates method. Int. J. Heat Mass Transfer 34 (1991) 2265–2273.
[30] M.F. Modest, Radiative Heat Transfer. McGraw-Hill, New York, 1993, pp. 541–571.
[31] B.G. Carlson, K.D. Lathrop, Transport theory—the method of discrete ordinates, in: H. Greenspan, C.N. Kelber, D. Okrent (Eds.), Computing Methods in Reactor Physics, Gordon and Breach Press, New York, 1968, pp. 165–266.